action. We conclude that the excluded-volume effect increases the strength of the low-frequency dispersion.

5. Summary

In this paper we have shown that the relative strength of the low-frequency, molecular-weight-dependent dielectric dispersion is given by the ratio Γ, defined in eq 1. This result is very general. It depends on an assumption of large molecular weight, sufficiently large that the unperturbed chain obeys Gaussian statistics and that the two dielectric dispersions are well separated in time or frequency domains. In particular it is valid for chains with arbitrary excluded-volume interactions including three-body and higher terms.

This result is consistent with what one would expect. Any chain for which $\langle \mu \cdot \mathbf{r} \rangle$ is zero will yield $\Gamma = 0$. Such chains are indeed expected[1-3] to exhibit only a single, relatively fast, molecular-weight-independent dielectric dispersion in dilute solution. On the other hand, chains for which the total dipole moment can be represented as due to two opposite and equal charges at opposite ends of the chain have $\Gamma = 1$. Such chains also exhibit a single dispersion, but one which is, in this case, slower and dependent on the molecular weight.[1-3] Chains with intermediate values of Γ display both dispersions. Note that Γ, by its definition, is limited to the range $0 \leq \Gamma \leq 1$.[4]

In addition, we predict, in eq 34, the excluded-volume behavior of Γ and observe that Γ increases with increasing excluded volume. Excluded volume acts to increase the strength of the low-frequency dispersion.

The experimental verification of theoretical predictions of the excluded-volume effect has always been rather difficult. This is because the quantity which is easiest to calculate, $\langle r^2 \rangle$, unlike R_g or $[\eta]$, has evaded direct experimental measurement. We note here, however, that the Nagai–Ishikawa–Doi formula relates $\langle r^2 \rangle$ directly to the measurable quantity $\langle \mu^2 \rangle$.

Acknowledgment. Partial support for this work has been provided by the National Science Foundation, Grant DMR-8607708.

References and Notes

(1) Stockmayer, W. H.; Baur, M. E. *J. Am. Chem. Soc.* **1964**, *86*, 3485.
(2) Baur, M. E.; Stockmayer, W. H. *J. Chem. Phys.* **1965**, *43*, 4319.
(3) Stockmayer, W. H. *Pure Appl. Chem.* **1967**, *15*, 539.
(4) Doi, M. *Polym. J.* **1972**, *3*, 252.
(5) Nagai, K.; Ishikawa, T. *Polym. J.* **1971**, *2*, 416.
(6) Vaughan, W. E. *Annu. Rev. Phys. Chem.* **1979**, *30*, 103.

Dispersion and Polydispersity Effects in the Transport of Xanthan in Porous Media

W. D. Brown* and K. S. Sorbie†

AEE Winfrith, Dorchester, Dorset, U.K. *Received February 3, 1988; Revised Manuscript Received December 7, 1988*

ABSTRACT: Recent experimental work on the flow of xanthan through nonadsorbing porous media has demonstrated a clear surface exclusion effect in which larger molecular weight species propagate faster than smaller fractions through the pore structure. Effluent measurements in these experiments include an assay for total polymer concentration and intrinsic viscosity of the produced solutions. Assuming zero hydrodynamic dispersion, these results may be analyzed using simple surface exclusion models to obtain the original molecular weight distribution (MWD) of the native polymer. In this paper, we model the transport of polymer through porous media using a multicomponent representation of the MWD, including the effects of hydrodynamic dispersion and surface exclusion. These calculations indicate that the data in such experiments are more difficult to interpret than the simple surface exclusion models alone would suggest. As a result of our calculations, supplementary experiments, necessary to clarify the interpretation, are suggested.

1. Introduction

Polymer transport in porous media is very important in a wide range of applications including polymer flooding in enhanced oil recovery (EOR), flow through membranes, and chromatographic columns. In describing the flow of polymers mathematically using macroscopic transport equations, a number of effects may have to be included in the formulation such as polymer dispersion, adsorption, excluded volume effects, chemical reactions, and viscous instabilities. In previous work on the modeling of polymer transport in porous media as it applies to EOR, the polymer has invariably been considered as a single-component species transported in the aqueous phase.[1-4] However, most polymers are polydisperse, and it is not expected that the transport properties of the lower and higher molecular weight species should be the same. Recently, experiments have been conducted by Lecourtier and Chauveteau[5,6] on the flow of xanthan through silicon carbide columns, which show that the single-component assumption is not adequate to describe polymer transport under all circumstances. In this work, Lecourtier and Chauveteau[5,6] showed that, in nonadsorbing porous media, the larger molecular weight species have a higher average pore velocity than smaller molecular fragments or tracer particles. They interpreted this as being due to entropic exclusion of the semirigid xanthan molecules from the walls of the pores,[5-8] with the larger molecules showing a stronger surface exclusion effect. They used these observations as the basis to obtain the molecular weight distribution (MWD) of the original polymer.

In this work, we investigate the transport modeling of polymer flow in porous media using a multicomponent

† Present address: Department of Petroleum Engineering, Heriot-Watt University, Riccarton, Edinburgh, Scotland.
* To whom correspondence should be addressed at BP Research Centre, Chertsey Rd, Sunbury-on-Thames, Middlesex, England.

0024-9297/89/2222-2835$01.50/0

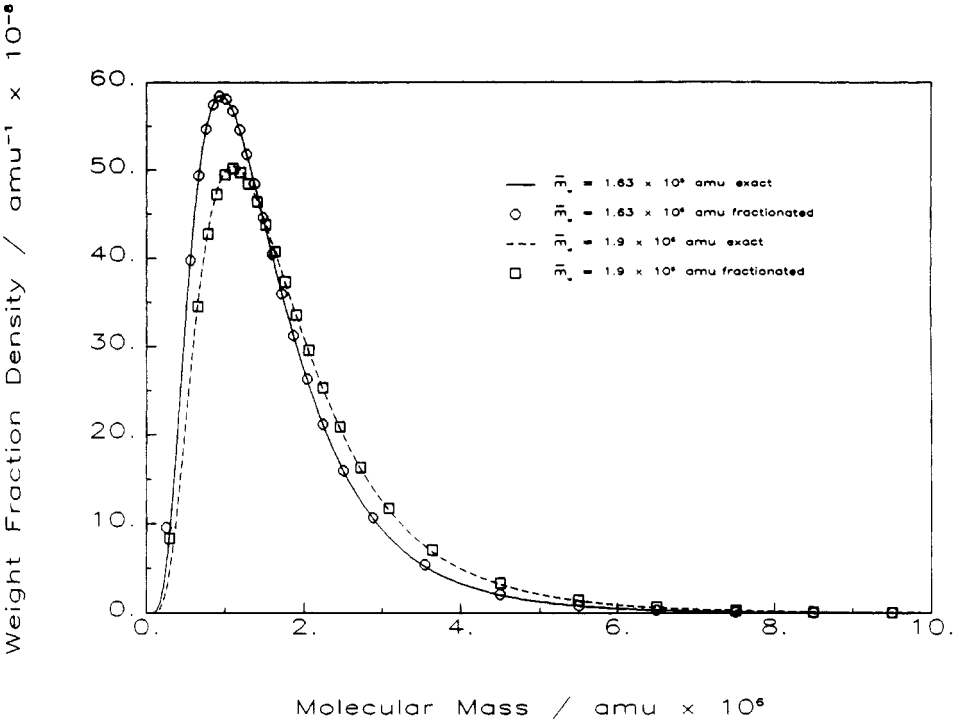

Figure 1. Wesslau distributions and their fractionated representation.

representation of the polymer to represent its MWD. The transport equations developed are then used to model and quantitatively interpret the Lecourtier and Chauveteau results. We show that the interpretation of their data is not straightforward due to the complex interaction of the effects of polydispersity, surface exclusion, and hydrodynamic dispersion. The observed phenomena are explained in detail, and further experiments are suggested, on the basis of our modeling work, which will help to clarify the interpretation of such experiments.

2. Models of Polymer Behavior

2.1. Surface Exclusion Models in Porous Media. In this section, we discuss a simple analysis of Auvray[8] and Lecourtier and Chauveteau[5,6] of the effect of surface exclusion on transport in porous media. An extension of this approach is then presented, which is used below.

For rods of length L the entropic surface exclusion at a flat wall reduces the concentration of rod centers $C(z)$ from the bulk value, C_0, at distances $z \leq L/2$ from the wall.

$$\begin{aligned} C(z) &= C_0 2z/L \qquad z \leq L/2 \\ &= C_0 \qquad z \geq L/2 \end{aligned} \tag{1}$$

In other geometries there will be a similar effect increasing concentrations away from walls and depleting those nearby. Since the fluid velocities of a solution in flow will in general be greater away from walls due to viscous effects, it follows that rods in solution will, on average, have a higher velocity relative to that of the solvent. In order to obtain an expression for velocity enhancement factors in porous media, Lecourtier and Chauveteau[5,6] considered the flow of rods in capillaries of radius R, assuming eq 1 to describe the rod concentration and the Poiseuille formula for the fluid velocity distribution

$$v(r) = \frac{1}{4\eta_0}(R^2 - r^2)\frac{dP}{d\lambda} \tag{2}$$

where $dP/d\lambda$ is the pressure gradient along the length of the capillary, r is the radial distance from its central axis, and η_0 is the viscosity of the fluid. The velocity is then averaged over the concentration to obtain

$$v_p = \left(\frac{1}{4\eta_0}\right)\left(\frac{dP}{d\lambda}\right) \times \frac{\int_0^R dr\, r(R^2 - r^2) - \int_{R-L/2}^R dr\, r\left(1 - \frac{2(R-r)}{L}\right)(R^2 - r^2)}{\int_0^R dr\, r - \int_{R-L/2}^R dr\, r\left(1 - \frac{2(R-r)}{L}\right)} \tag{3}$$

Table I
Fractionation Scheme for Two Wesslau Distributions

component no.	$\bar{m}_w = 1.63 \times 10^6$ amu: mass, 10^6 amu	$\bar{m}_w = 1.63 \times 10^6$ amu: wt fractn, %	$\bar{m}_w = 1.9 \times 10^6$ amu: mass, 10^6 amu	$\bar{m}_w = 1.9 \times 10^6$ amu: wt fractn, %
1	0.252	4.8	0.296	4.9
2	0.565	4.8	0.663	4.9
3	0.674	4.8	0.793	4.9
4	0.767	4.8	0.903	4.9
5	0.853	4.8	1.005	4.9
6	0.937	4.8	1.104	4.9
7	1.019	4.8	1.203	4.9
8	1.103	4.8	1.304	4.9
9	1.190	4.8	1.408	4.9
10	1.280	4.8	1.518	4.9
11	1.377	4.8	1.635	4.9
12	1.481	4.8	1.761	4.9
13	1.594	4.8	1.901	4.9
14	1.721	4.8	2.059	4.9
15	1.865	4.8	2.240	4.9
16	2.034	4.8	2.457	4.9
17	2.240	4.8	2.727	4.9
18	2.505	4.8	3.089	4.9
19	2.882	4.8	3.650	4.9
20	3.554	4.8	4.5	3.4
21	4.5	2.1	5.5	1.5
22	5.5	0.8	6.5	0.7
23	6.5	0.4	7.5	0.3
24	7.5	0.2	8.9	0.2
25	8.5	0.1	9.5	0.1
26	9.5	0.04		

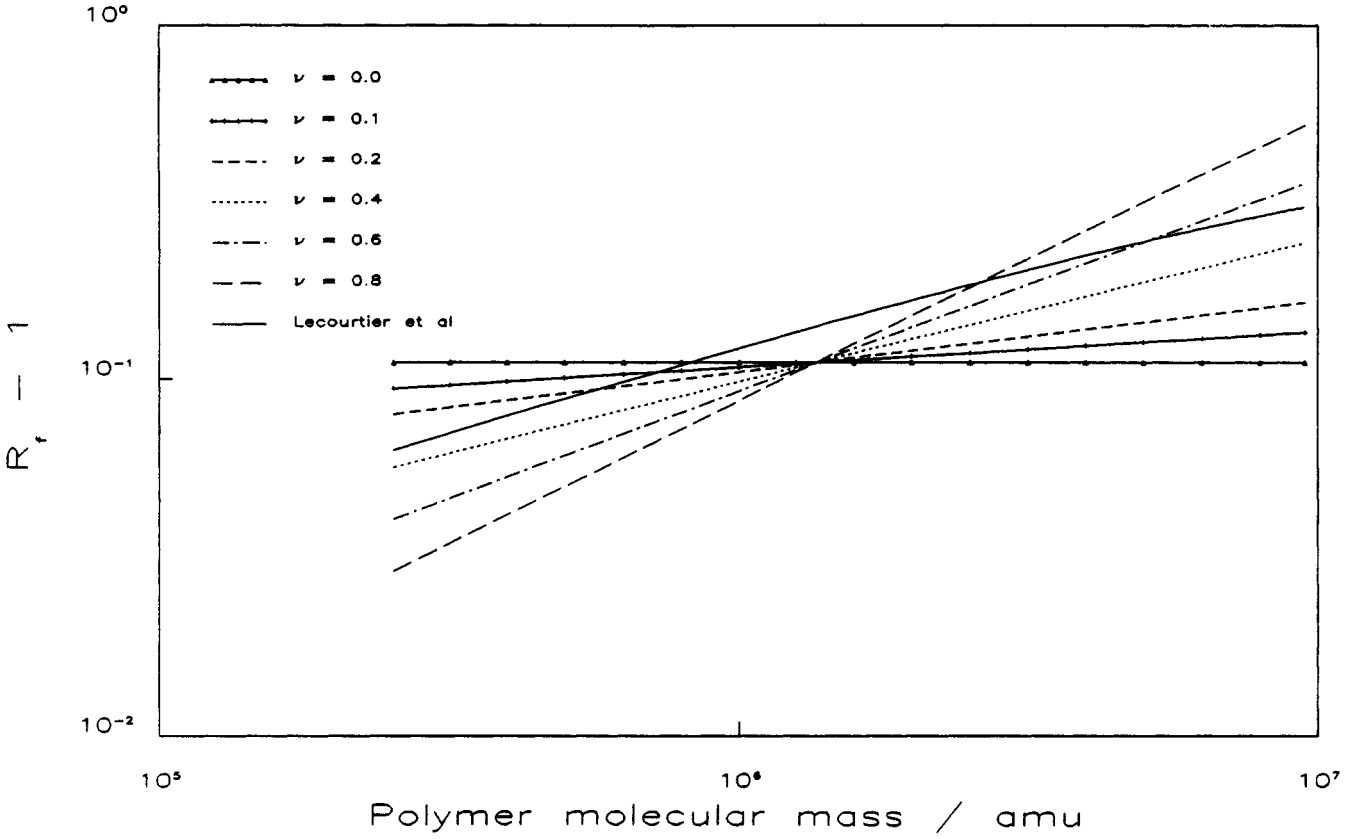

Figure 2. Molecular mass dependence of polymer advancement.

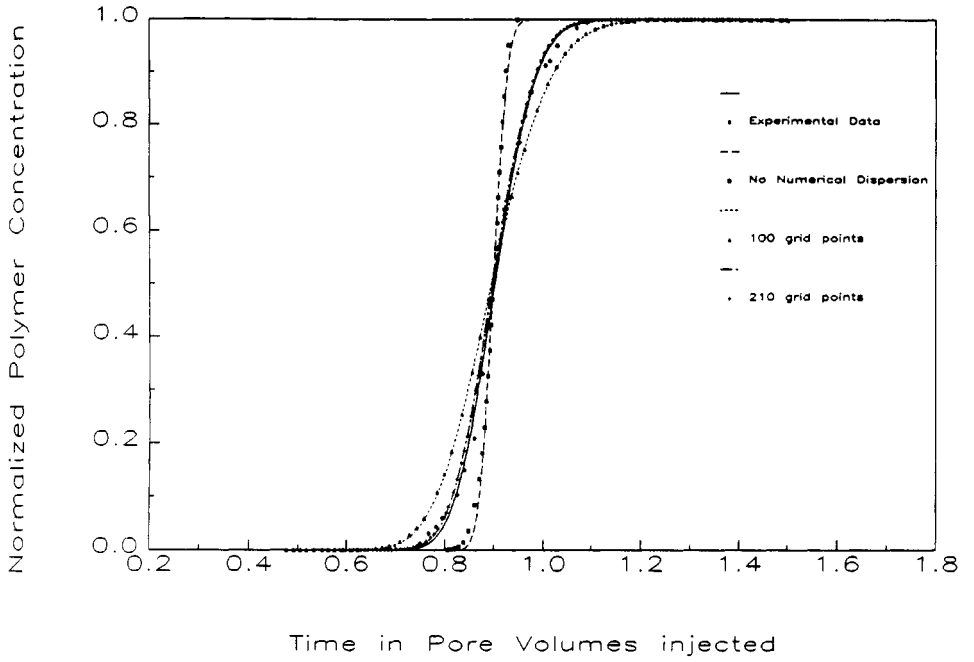

Figure 3. Experimental matching procedure for $\nu = 0.4$.

The correctness of this formula depends upon the rod length, L, being smaller than the tube radius, R (so that the surface exclusion formula is correct), and on the velocities being low so that molecular orientational effects are not significant.

The application of this result to the flow of rodlike polymers in porous media requires the identification of an average hydrodynamic length of the rod, L_{eq}, and of an effective capillary size of the porous medium, R_{eff}. The first parameter was taken to be the length of the ellipsoids, which would yield the same viscosity as the polymer, if in solution at the same concentration. This yielded a dependence on polymer mass of $L_{eq} = \alpha m^{\nu}$. The second parameter, R_{eff}, was taken as a fitting parameter.

Equation 3 may be expanded as a power series in L_{eq}/R_{eff} and related to velocity enhancement factors, R_f, defined such that the velocity of polymer, v_p, is related to the fluid velocity, v_f, by $v_p = R_f v_f$, giving

$$R_f = 1 + \mu m^{\nu} + \ldots \tag{4}$$

where $\nu = 0.93/1.812 \simeq 0.5$.

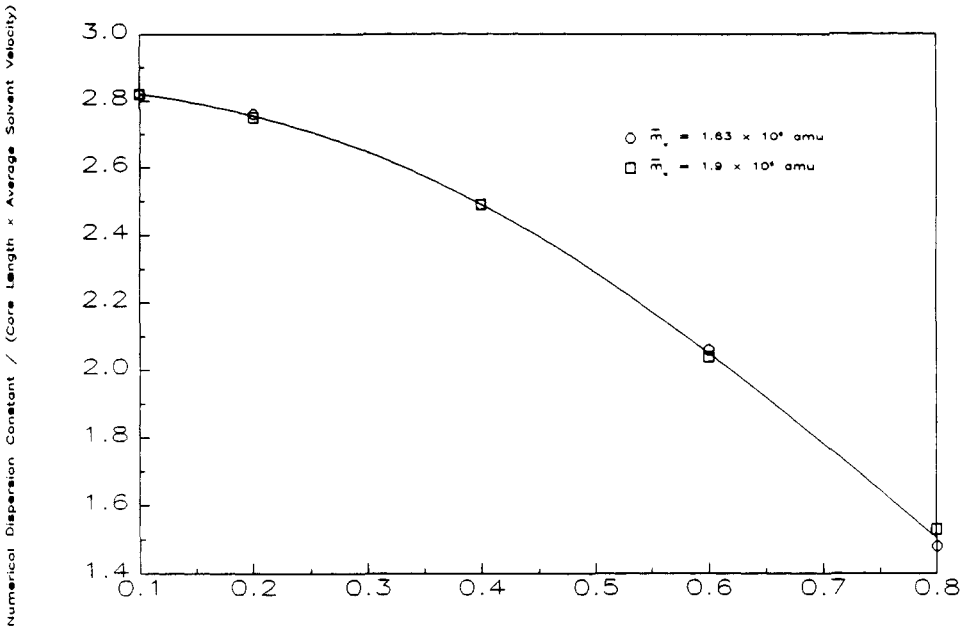

Figure 4. Values of hydrodynamic dispersion matching different amounts of surface exclusion.

While this approach is very attractive in that it captures two of the essential features of the surface exclusion effect in porous media, there is reason to doubt its correctness in detail. In particular the value of ν is determined by an ellipsoidal model of the xanthan molecules. It thus makes very particular assumptions about molecular configurations. Accordingly, in our work, we assume a form of the type of eq 4 but leave the exponent general. We note that, in the above approach, a specific value of R_f is assigned to a molecule of a given size. If we have a distribution of polymer masses the formula will indicate the corresponding range of R_f's that will be observed, with the larger polymers moving more quickly. Identifying an average value of the velocity enhancement factor, $\bar{R}_f$, and associating it with an average mass, m_0, our general expression is written as

$$R_f = 1 + (\bar{R}_f - 1)(m/m_0)^\nu \tag{5}$$

In order to apply this procedure to the transport of polydisperse polymers, we must define a suitable MWD, and this is discussed in the following section.

2.2. Molecular Weight Distribution. For many types of polymer solution, the distribution of molecular weights may be determined on an a priori basis, using an understanding of the kinetics of the polymerization process (for example, Flory–Stockmayer theory[9]). However, for biopolymers it is not clear how to proceed in this way. In this paper, we use the empirical form of the Wesslau distribution,[10] which defines a log–normal molecular weight fraction distribution, $C(m)$, as

$$C(m) = \frac{1}{\sqrt{\pi}} \frac{1}{\gamma m} \exp\{-[\ln^2 (m/m_0)/\gamma^2]\}$$

with

$$\gamma^2 = \ln (I_p^2)$$
$$m_0 = [\bar{m}_w \cdot \bar{m}_n]^{1/2} \tag{6}$$
$$I_p = \bar{m}_w/\bar{m}_n$$

where $\bar{m}_w$ and $\bar{m}_n$ are the weight- and number-average molecular weights, respectively, and I_p is the polydispersity index. It is not difficult to show that this definition of m_0 is consistent with that of section 2. This form of the mass distribution was the one reported by Lecourtier and Chauveteau[5,6] for xanthan albeit on the basis of an analysis that we will later question.

In order to calculate the effects of transport in a porous medium on the MWD, it is necessary to discretize the distribution as shown in Figure 1. In this discretization, a number of practical points must be considered. The number of components must be chosen in order to represent the MWD adequately, but this must not be impractically large for transport modeling. We must also choose a suitable upper mass cutoff for the discretized distribution. In one application that was made of the discretized distribution moments were required up to order 1.5. Accordingly, care had to be taken with the representation of the high mass end of the distribution. The midpoint of the discretized mass fractions was taken to represent the entire component, and all properties, such as velocity enhancement factor and intrinsic viscosity of the component, were calculated using this value of molecular weight.

The scheme that was used in this work disregarded masses above 10^7 amu, thus discounting the top 0.05% by weight of the distribution. Totals of 25 and 26 fractions were used in the examples taken, these being apportioned as shown in Table I, with equal weight fractions at the lower end and equal mass windows at the top.

2.3. Intrinsic Viscosity of Polymer MWD. We now consider the calculation of the intrinsic viscosity of a given MWD. The intrinsic viscosity $[\eta]_0$ of a polydisperse polymer solution may be written quite generally as

$$[\eta]_0 = \int_0^\infty dm\ C(m)\ [\eta]_0(m) \tag{7}$$

where $[\eta]_0(m)$ is the intrinsic viscosity associated with a solution of monodisperse polymer of molecular weight, m. The intrinsic viscosity, $[\eta]_{0i}$, may be found from the Mark–Houwink relation for the ith species of molecular

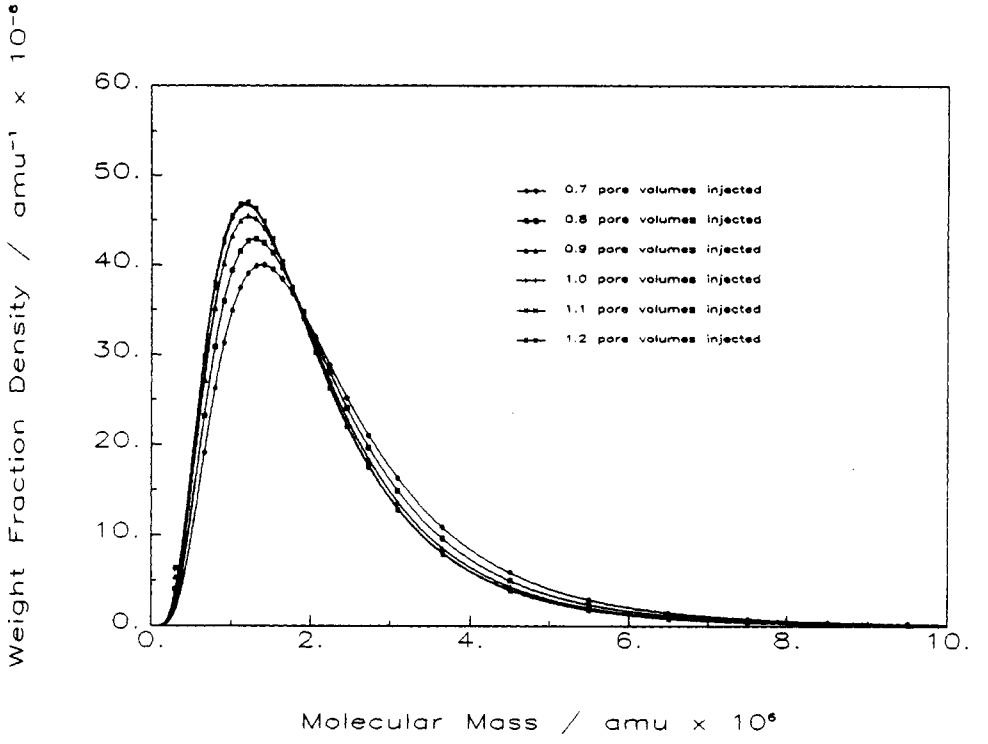

Figure 5. Effluent mass distributions at successive times for $\bar{m}_w = 1.9 \times 10^6$ amu and $\nu = 0.1$.

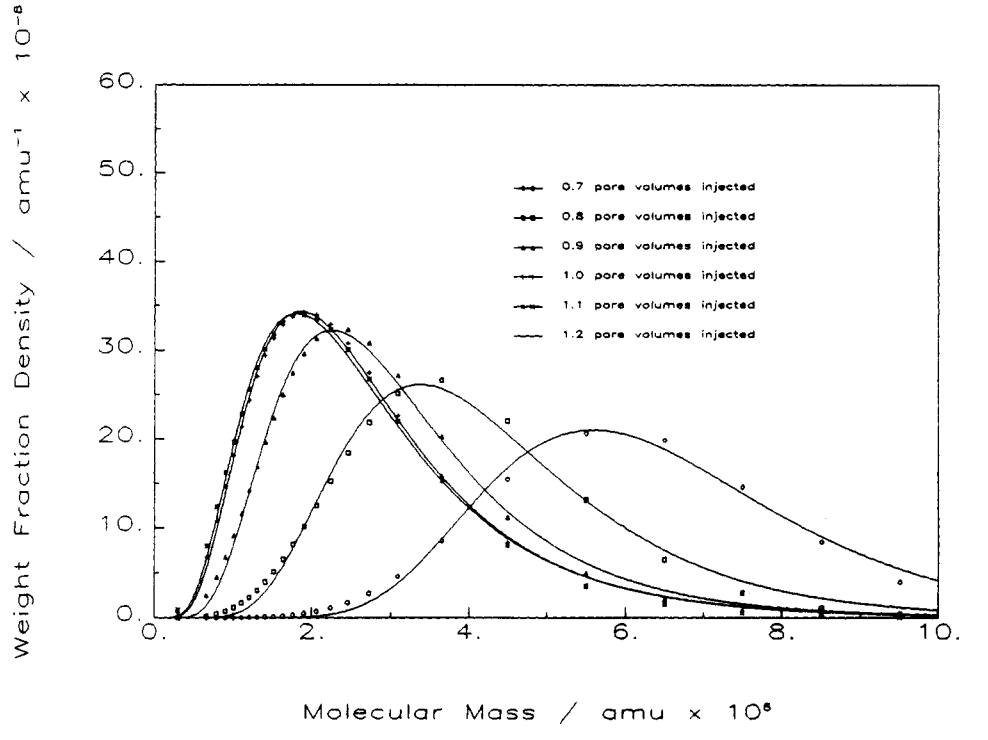

Figure 6. Effluent mass distributions at successive times for $\bar{m}_w = 1.9 \times 10^6$ amu and $\nu = 0.8$.

weight, m_i, in a MWD and may be written

$$[\eta]_{0i} = \alpha m_i^{\beta} \tag{8}$$

If we now assume the following general scaling form for the mass distribution

$$C(m) = m^{-1} g(m/\bar{m}_w) \tag{9}$$

where $g(\xi)$ is a function of the scaling variable ξ then

$$[\eta]_0 = \alpha' \bar{m}_w^{\beta} \tag{10}$$

Thus, if a set of polydisperse solutions obey a Mark–Houwink type relation, it seems reasonable that they should have a distribution of the type of eq 9. The Wesslau distribution is a particular example of this for which

$$[\eta]_0 = I_p^{\beta(1-\beta)/2} \cdot \alpha \bar{m}_w^{\beta} \tag{11}$$

For β close to unity the constant of proportionality is close to the monodisperse value. In fact, the correction factor for xanthan (which has a Mark–Houwink exponent, $\beta = 0.93$[11]), with an assumed $I_p = 1.4$, is 2% and is, furthermore, insensitive to changes in the polydispersity.

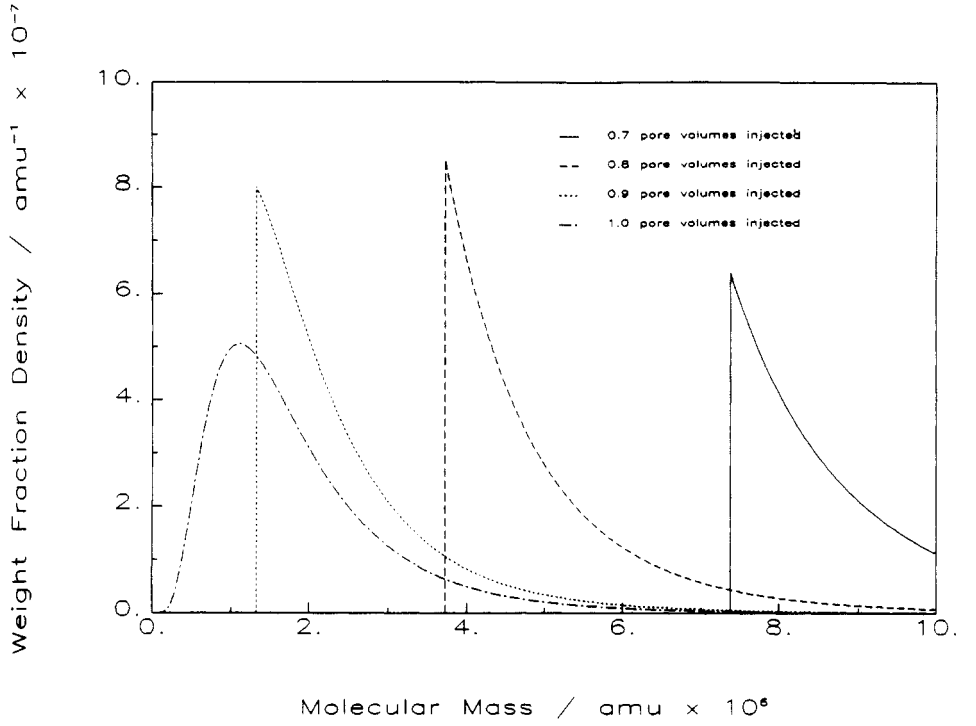

Figure 7. Nondispersive effluent mass distributions at successive times for $\bar{m}_w = 1.9 \times 10^6$ amu.

3. Transport Equation for Multicomponent Polymers

The behavior of polymers in porous media is complex. However, by restricting our attention to the displacement of water by dilute polymer solution, complications such as viscous instabilities disappear. The cases considered here do not show adsorption or reaction, consistent with the studies of Lecourtier and Chauveteau.[5,6] The transport behavior that remains may be modeled solely by the convective dispersion equation in which components show only dispersive and surface exclusion effects as

$$\partial C_i/\partial t = \nabla(D_i \nabla C_i) - v_i \nabla C_i \qquad (12)$$

where C_i is the concentration of the ith polymer fraction, v_i its velocity, and D_i its associated hydrodynamic dispersion coefficient in the porous media.

This equation is the one used in our work to model polymer flow in porous media, with the injected polymer MWD given by the Wesslau function and the component velocities, v_i, being determined by the model proposed in section 2.1. The geometry was one dimensional with the input boundary maintaining constant concentrations of the polymer fractions and the exit boundary at $x = \lambda$ draining convectively

$$\frac{\partial C}{\partial t}(x=\lambda) = -v\frac{\partial C}{\partial x}(x=\lambda) \qquad (13)$$

The effect of this boundary was found to be virtually identical with maintaining the concentrations at zero at a large (effectively infinite) distance away from the input.

In order to solve the transport equations numerically, the method of lines[12,13] was used with single-point upstreaming[14] of the convective terms. This single-point discretization procedure gives rise to diffusive numerical errors, which were then used to model the dispersion terms (D_i). Efficient time integration in the method of lines meant that the numerical dispersion could reliably be predicted by the formula in eq 14 where Δx was the mesh size used in the spatial discretization of eq 12.

$$(D_i)_{num} = v_i \Delta x/2 \qquad (14)$$

This dispersion can of course be altered simply by refining or coarsening the spatial grid. The discretized version of eq 12 had D set to zero, and solely numerical dispersion was used to model the D of the continuum equation.

4. Results and Comparison with Experiment

4.1. Lecourtier–Chauveteau Experiment. Use of the above mathematical model was made to simulate one of the experiments reported by Lecourtier and Chauveteau.[5,6] In this experiment, 200 ppm xanthan solution was continuously injected into a core of a porous medium of length 0.65 m and cross-sectional area 5.7×10^{-4} m^2, formed from packed 18-μm SiC spheres. (It should be noted that the polymer solution was prepared at low concentration and high salinity under carefully controlled conditions, both microgels and low molecular weight impurities being removed and bactericide added.) Both the total polymer concentration and intrinsic viscosity of the effluent solution were recorded as functions of time measured in pore volume throughput of fluid. This was taken as the basis for an analytical method to determine the molecular weight distribution of xanthan.

Lecourtier and Chauveteau's[5,6] interpretation of this experiment was carried out solely by making use of eq 3 and a Mark–Houwink relation for the effluent intrinsic viscosities, thus neglecting any effect that dispersion might have. In this section, we shall demonstrate that this is not sufficient to determine the MWD under the experimental conditions used and shall go on to suggest a technique that may be more appropriate.

Two sets of computational studies were carried out using two injected polymer solutions, which had weight-average molecular weights of $\bar{m}_w = 1.63 \times 10^6$ and 1.9×10^6 amu; both had polydispersities of $I_p = 1.43$. These values of molecular weight were chosen to lie on either side of the value quoted by Lecourtier and Chauveteau (1.8×10^6 amu) since there appeared to be some uncertainty over this

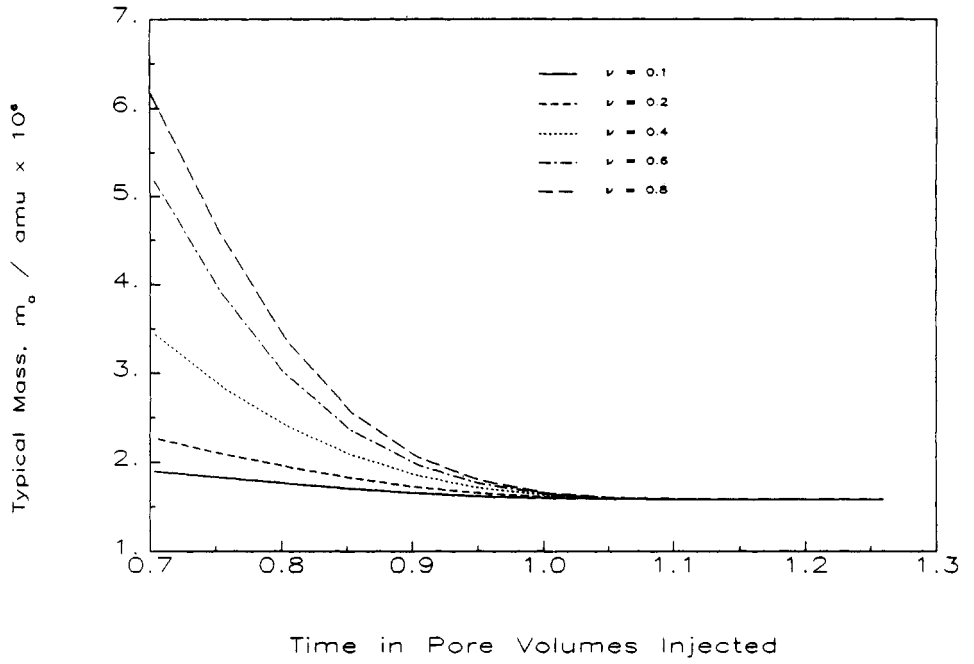

Figure 8. m_0 against time for different surface exclusions ($\bar{m}_w = 1.9 \times 10^6$ amu).

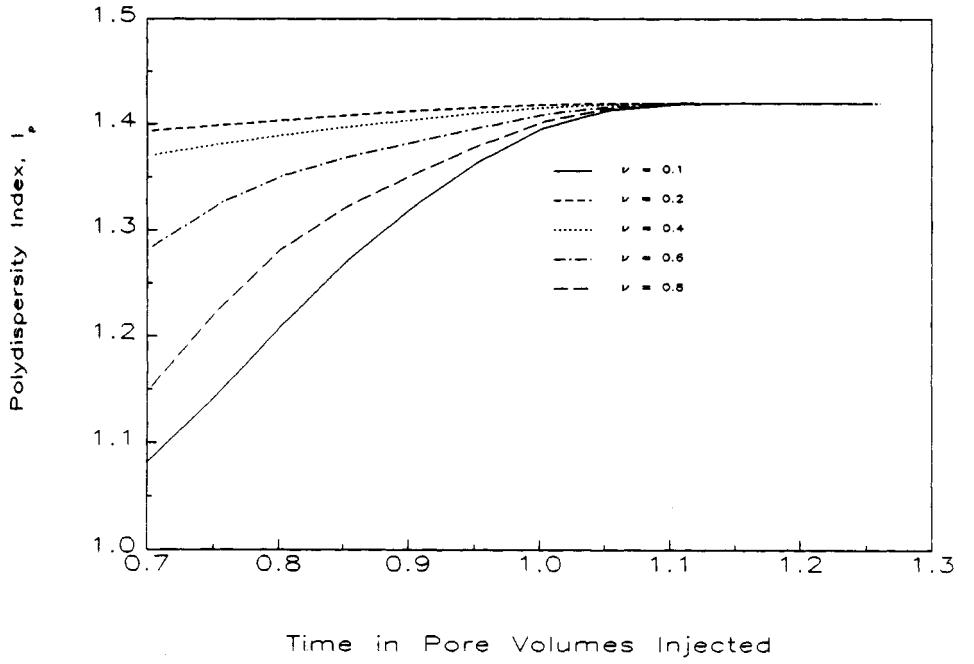

Figure 9. I_p against time for different surface exclusions ($\bar{m}_w = 1.9 \times 10^6$ amu).

value. The molecular weight distributions for polymers were taken to be Wesslau distributions, as discussed above, and are shown in Figure 1. These MWD's are completely defined by the two parameters $\bar{m}_w$ and I_p. Values were also attributed to the transport parameters D_i and v_i, defined in eq 11. The latter was determined by ν and the component mass as in eq 5. This dependence on the mass is shown in Figure 2, for each of the values of ν taken, in terms of velocity enhancement factors, R_f. The dependence obtained by Lecourtier and Chauveteau, in section 2, is given for comparison. In this way velocities and dispersivities were assigned to each polymer mass in the distribution.

4.2. Matching Total Effluent Concentration. Cases with a range of values of ν were investigated. For each case there was found to be a correct amount of dispersion that would reproduce the experimental effluent profile for the total polymer concentration as a function of time. That is, the spread in the effluent profile is attributed to a combination of hydrodynamic dispersion and the separation of different molecular weight components due to surface exclusion effects (parametrized by ν). An example of the procedure used is shown in Figure 3 for $\bar{m}_w = 1.63 \times 10^6$ amu and $I_p = 0.4$. For the level of frontal spreading associated with $\nu = 0.4$, it was found that we required the additional numerical dispersion associated with 224 grid points in order to fit the total effluent concentration profile. This value was obtained by performing computational floods for various numbers of grid points. Purely dispersive analytical solutions[15] were then fitted to each calculated profile, and each was characterized by a Peclet number accordingly. As a Peclet number has been similarly inferred for the experimental flood, it was a matter of interpolation to deduce the number of grid points ap-

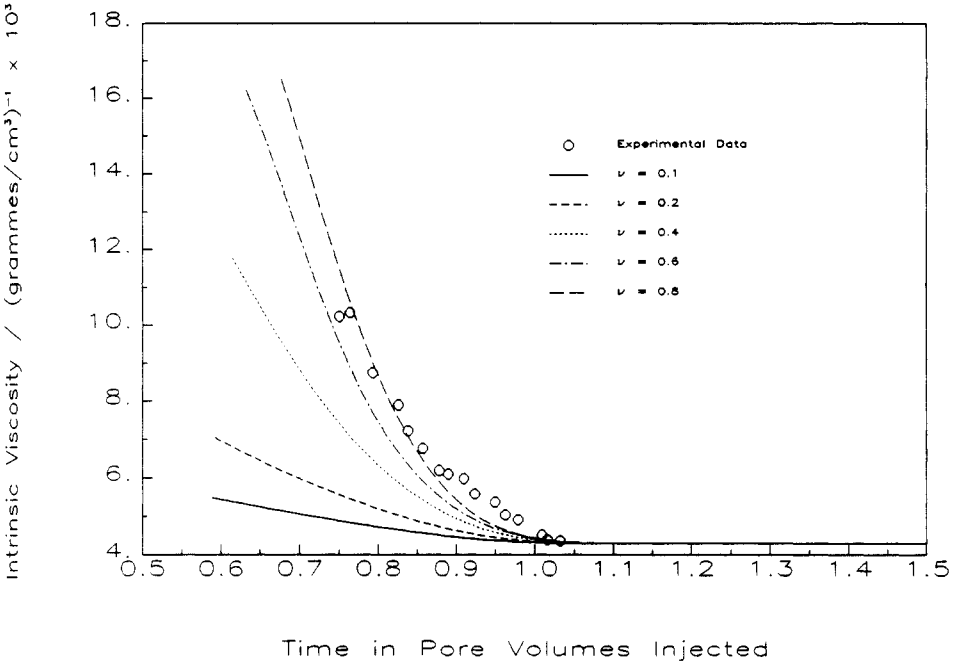

Figure 10. Effluent intrinsic viscosity for $\bar{m}_w = 1.63 \times 10^6$ amu.

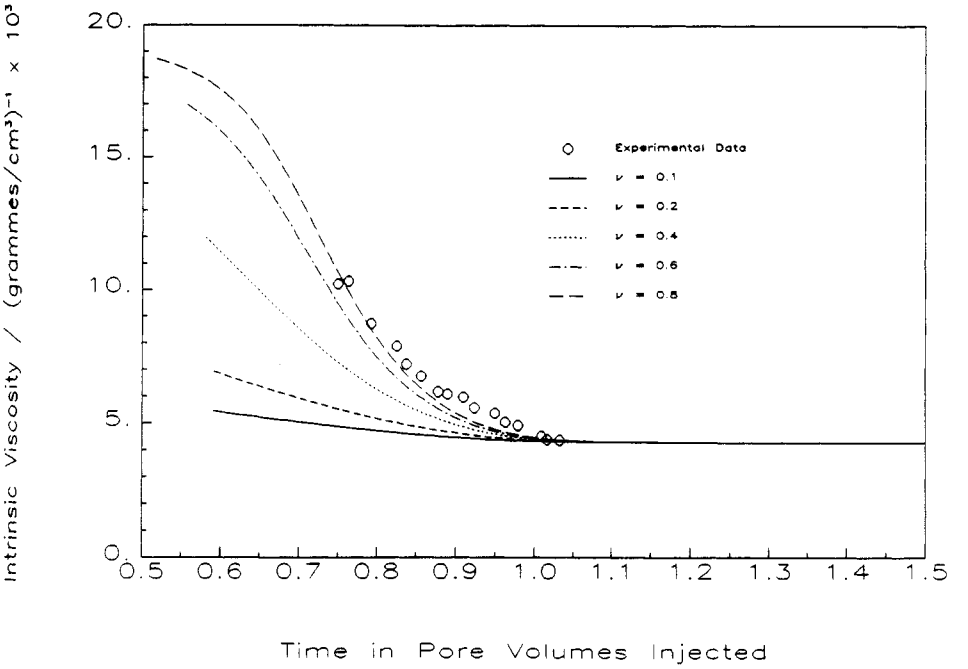

Figure 11. Effluent intrinsic viscosity for $\bar{m}_w = 1.9 \times 10^6$ amu.

propriate to the physical dispersion for any assumed value of ν. It should be noted here that fits could not be obtained by varying D for values of ν as large as 0.9 since this would imply measurable concentrations of polymer leaving the core at times earlier than observed in experiment, even without added dispersion.

In this way functions $D(\nu)$ were identified that gave satisfactory fits to the total effluent polymer concentration profiles. Plots of these functions are presented for the two values of influx average molecular weights taken in Figure 4. Quantitatively, these indicate how the total dispersion of a polymer front may be apportioned between chromatographic effects in which polymers of different masses separate and hydrodynamic dispersion, which causes the separation of polymers of identical masses. It is clear from Figure 4 that the magnitude of dispersion (D) and surface exclusion effects (ν) are, as we expect, inversely related for a given experimental effluent fit. That is, the more dispersion that is included in the calculation, the less spread that needs to be included through surface exclusion effects in order to obtain a good fit to the experimental data and vice versa. Clearly, the whole picture cannot be deduced from total concentration profiles alone. Information on the intrinsic viscosity measurements on effluent samples must also be included in order to distinguish between various D, ν combinations that fit total concentrations.

4.3. Modeling Intrinsic Viscosity Profiles. Examination of how the effluent mass distributions evolve in time within our computational study shows there to be marked differences between the cases $\nu = 0.1$ and $\nu = 0.8$ for each value of m taken. Calculated effluent MWD's for $\bar{m}_w = 1.9 \times 10^6$ amu are shown in Figures 5 and 6 for cases with low ($\nu = 0.1$) and high ($\nu = 0.8$) levels of surface exclusion effect respectively. As we expect, the average

Table II
Table Showing the Time in Pore Volumes Injected, T, up to Which Effluent Was Collected and the Values of m_0 and I_p for the Resultant Solutions, with the Influx Solution Having a Weight-Average Molecular Weight of the Following

ν	T, pore vols injd	m_0, 10^6 amu	I_p
	$\bar{m}_w = 1.63 \times 10^6$ amu		
0.1	0.867	1.447	1.423
0.2	0.868	1.541	1.414
0.4	0.867	1.728	1.386
0.6	0.864	1.896	1.332
0.8	0.868	2.077	1.250
	$\bar{m}_w = 1.9 \times 10^6$ amu		
0.1	0.871	1.681	1.410
0.2	0.877	1.765	1.401
0.4	0.866	2.013	1.369
0.6	0.867	2.181	1.318
0.8	0.865	2.358	1.264

molecular weight of successive effluent fractions for the $\nu = 0.1$ case (Figure 5) changes very little; thus, we would expect the effluent intrinsic viscosity to change little with time in this case. In contrast, in the $\nu = 0.8$ case shown in Figure 6, the average molecular weight of earlier effluent samples is considerably larger than later ones. This latter case, as we will see below, gives early effluents with higher intrinsic viscosities than later effluents. Comparison with Figure 7, which shows the equivalent nondispersive cases, highlights the importance of dispersion. In order to clarify the effect of the surface exclusion parameter, ν, on the properties of effluent samples, the time evolution of the polydispersity index, I_p, and "typical mass", m_0, were calculated. Both I_p and m_0 were calculated numerically from the moments of the predicted MWD profile (based on relative quantities of the 26 components) and are defined as

$$I_p = (\overline{m^2}_w)/(\bar{m}_w) \tag{15}$$

and

$$m_0 = \frac{\bar{m}_w}{\sqrt{I_p}} \tag{16}$$

The results for all nonzero values of ν are recorded in Figures 8 and 9. These measures of the polydispersity and of a typical mass in the distribution were chosen on the grounds of numerical stability. Although these values will equal those defined in eq 6 for the influx distribution, this equivalence depends upon the moments of the mass distribution scaling and cannot in general be taken to hold.

The measurement of intrinsic viscosity as performed by Lecourtier and Chauveteau is one means by which the evolution of effluent mass distributions may be recorded. However, from a given value of intrinsic viscosity we may only calculate a value of $\bar{m}_w$ for the particular effluent sample and *not* the molecular weight distribution. In order to obtain this MWD experimentally, we must correctly interpret and model the transport processes (both surface exclusion *and* dispersion effects) within the porous medium. Effluent intrinsic viscosities were calculated in the computational floods on the basis of eq 7 and 8 and are shown in Figures 10 and 11 for the lower and the higher molecular weight species, respectively. In order to take account of the experimental intrinsic viscosity of the influx solution being consistent only with $\bar{m}_w = 1.9 \times 10^6$ amu for the standard Mark–Houwink parameters, α was altered in the $\bar{m}_w = 1.63 \times 10^6$ amu floods to give the correct value for the initial solution. In all cases the amount of dispersion required to fit the concentration profile was taken.

Table III
Values of the Average Velocity Advancement Factor, $\bar{R}_f$, and Peclet Number, P_e, on First and Second Injections

		first pass		reinjection	
$\bar{m}_w$, 10^6	ν	$\bar{R}_f$	P_e	$\bar{R}_f$	P_e
1.63	0.1	1.11	391	1.11	392
	0.8	1.11	300	1.16	283
1.9	0.1	1.11	391	1.11	392
	0.8	1.11	300	1.16	283
expt		1.11	389		

It can be seen that the best intrinsic viscosity fits are obtained for the cases in which $\nu = 0.8$. It is only at this relatively high value of ν that there is sufficient advancement of high molecular weight components to cause the observed spreading of intrinsic viscosity in the experiment. However, with the undoubted experimental difficulties in the measurement of $[\eta]_0$ and for corroboration, it would be useful to have another technique.

4.4. Alternative Experimental Technique. An alternative experimental approach that would help to distinguish between the contributions of dispersion and surface exclusion will now be discussed. The main idea in this technique is to collect a bulk sample of the early effluent just after the polymer breakthrough and to reinject this sample in a similar manner to the original experiment, i.e., measure effluent concentration and intrinsic viscosity profiles, etc. If dispersion dominates, then we would expect little further separation of molecular weight components as measured by intrinsic viscosity. However, if surface exclusion effects are very significant and differ sufficiently widely between molecular weight components, then further separation of components will again be seen in the reinjection experiment. Thus, the observations from this type of experiment would allow a much better definition of ν than the single-injection experiment. This experiment is now modeled, and the expected effects are quantified below.

The theoretical procedure followed in our study was as follows where all of the procedures in this section describe *numerical* experiments.

(i) Effluent was collected from (computational) floods as soon as the polymer concentration had reached 1% of that being injected; this would represent a small but measurable value for influx concentrations of 200 ppm.

(ii) The collection was continued until the polymer concentration of cumulatively collected effluent had reached 10% of the influx. The times up to which effluent had to be collected and the values m_0 and I_p of the resulting solution are recorded in Table II, with m_0 and I_p being defined in eq 15 and 16.

(iii) This collected effluent was then reinjected into the original core in its initial state. Reinjection was calculated for $\nu = 0.1$ and 0.8 both initial solution types using an amount of dispersion close to value appropriate to ν and identical with that used on the first pass.

Marked differences were now observed in the total effluent concentration profiles. This is clearly seen in Table III which records the effective values of the average polymer advancement factor, R_f, and of the effective Peclet number, P_e, as determined by an error function fitting routine, alongside those of the original injection process and experiment. It will be noted that while R_f and P_e are substantially unchanged for the lower value of ν, $\bar{R}_f$ is noticeably higher on reinjection for $\nu = 0.8$. As before there are definite distinctions to be seen in the intrinsic viscosity (Figure 12), with the higher value of ν showing the sharper profile of the two and descending to the higher final value. This latter point is in contrast with what happened on the

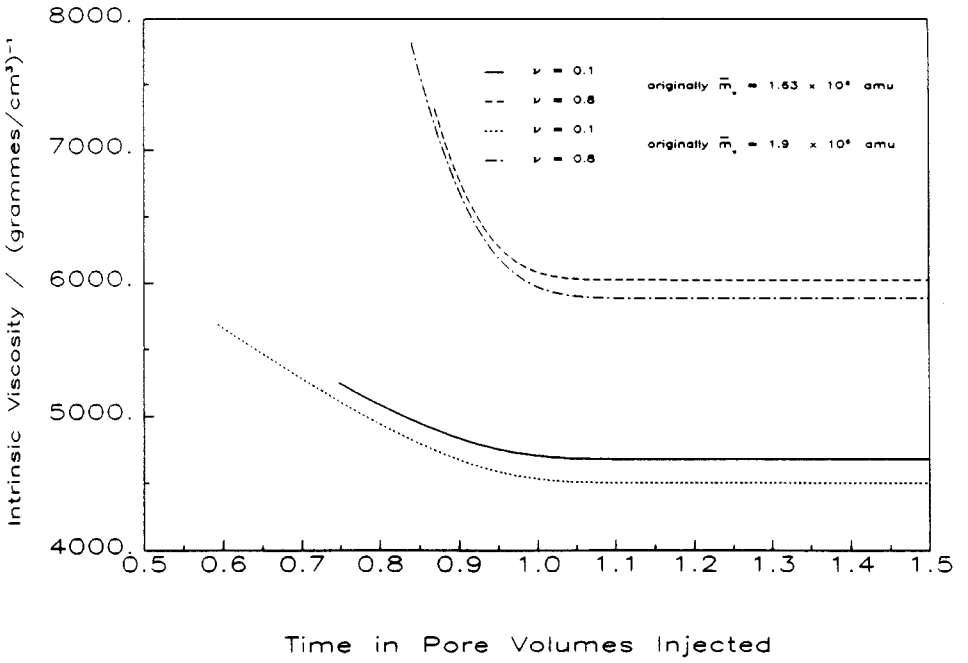

Figure 12. Effluent intrinsic viscosity for bulked influx solution.

first pass but is of course expected as the influx mass distributions in the reinjection cases are different for different values of ν.

5. Discussion and Conclusions

In this paper, we have demonstrated the importance of dispersion in interpreting the flow of polymer solutions through porous media where surface exclusion separation of molecular components occurs. Effluent total concentration profiles can be matched for any amount of frontal spreading due to surface exclusion effects (within limits) by adding dispersion. The additional matching of experimental intrinsic viscosity profiles identified a particular amount of velocity dispersion that was required. The velocity advancement factors taken were in all cases physically reasonable, lying between 1.0 and 1.5. The upper case corresponds to effective porosities in the experiment of Lecourtier and Chauveteau of slightly over 30% (where the pack porosity is ~47%).

This identification of ν was, however, slightly unclear as the measurement of intrinsic viscosities necessarily involves considerable experimental errors. Another means by which ν could be deduced was therefore proposed, whereby the core would be reflooded with bulked fractions collected from parts of the frontal profiles of an earlier flood. In this procedure, close agreement between the effluent concentration profiles seen in the initial and in the subsequent injection was shown to indicate a low value of ν. On the other hand, a higher value is indicated by an advancement of the profile, the precise degree of which defines ν.

The initial procedure of pairing a hydrodynamic dispersion D with each ν in order to match the effluent concentration profile was carried out successfully for two different computational molecular weight distributions. The intrinsic viscosities could furthermore be matched by altering the constant of proportionality in the Mark–Houwink relation, accordingly.

It is clear that the overall effect of dispersion is to convolve information about the mass distribution. Only if this dispersion can be reduced can useful interpretation be made of effluent concentration profiles. One possible means by which this could be done is by lengthening the

Table IV
Table Showing the Lengths of Cores That Would Be Required To Produce a Polymer Mass Separation ($r = \Delta m/m_0$) of 0.25 for Various Values of ν and Molecular Weight

ν	N_f	$\nu\sqrt{N_f}$	λ/λ_f (r = 0.25)
	$\bar{m}_w = 1.63 \times 10^6$ amu		
0.1	198	1.407	19.0
0.2	202	2.843	9.5
0.4	224	5.987	7.5
0.6	271	9.877	2.8
0.8	377	15.533	1.8
	$\bar{m}_w = 1.9 \times 10^6$ amu		
0.1	198	1.407	19.0
0.2	203	2.850	9.5
0.4	224	5.987	4.5
0.6	273	9.914	2.8
0.8	365	15.284	1.8

core. We now estimate the length of core that would be required with the two different mass distributions and with different values of ν in order to perform a chromatographic analysis. Clearly, for larger ν, we would expect that shorter cores may be employed since the velocity differences between components will be larger.

Two mass fractions $(m - \Delta m/2)$ and $(m + \Delta m/2)$ whose average velocities differ by Δv and whose dispersion constants are $D(m)$ will be resolved in time t if $\Delta vt \sim \sqrt{(Dt)}$. Equivalently, a length of core may be identified as the controlling parameter, giving

$$\lambda \simeq Dv/(\Delta v)^2 \tag{17}$$

If we now define the mass resolution, which is required, as Δm, the length of core needed is

$$\lambda(\Delta m) = \left[\frac{\bar{R}_f D(m_0)}{(\bar{R}_f - 1)^2 \nu^2}\right]^{1/2} \frac{m_0}{\Delta m} \tag{18}$$

D has already been determined in our (D, ν) matching procedure. Since it is given by the numerical dispersion formula (eq 14), it follows that

$$\frac{\lambda}{\lambda_f} = \left[\frac{\bar{R}_f}{2(R_f - 1)^2}\right]^{1/2} \frac{1}{\nu\sqrt{N_f}} \frac{m_0}{\Delta m} \tag{19}$$

where λ_f is the length of the core in the reported experiment and N_f was the number of grid points needed to yield the correct amount of dispersion.

The foregoing formula has been enumerated for a relative resolution, $r = \Delta m/m_0$, of 0.25 for the two mass distributions and range of ν values that have been used. These are tabulated in Table IV. If the physical value of ν actually is 0.8, then it can be seen that this is encouraging for future experiments as core lengths of 0.65 m × 1.8 = 1.2 m should begin to give results that are open to chromatographic interpretation.

Acknowledgment. This work was funded by the U.K. Department of Energy as part of its Enhanced Oil Recovery Programme.

Registry No. Xanthan gum, 11138-66-2.

References and Notes

(1) Sorbie, K. S.; Parker, A.; Clifford, P. J. 60th SPE Annual Fall Conference, Las Vegas, NV, Sept 1985; SPE 14231.
(2) Patton, J. T.; Coats, K. H.; Colegrove, G. T. *SPEJ* **1971**, March, 72–84.
(3) Bondor, P. L.; Hirasaki, G. J.; Tham, M. J. *SPEJ* **1972**, *Oct*, 369–382.
(4) Vela, S.; Peaceman, D. W.; Sandvik, E. I. 49th Annual Fall Conference, Houston, TX, Oct 1974; SPE 5102.
(5) Lecourtier, J.; Chauveteau, G. *Macromolecules* **1984**, *17*, 1340.
(6) Lecourtier, J.; Chauveteau, G. 59th Annual Technical Conference, Houston, TX, Sept 1984; SPE 13034.
(7) Chauveteau, G. *J. Rheol.* **1982**, *26*, 111–142.
(8) Auvray, L. *J. Phys. (Les Ulis, Fr.)* **1981**, *42*, 79–95.
(9) Flory, P. J. *Principles of Polymer Chemistry*; Cornell University: Ithaca, NY, 1953.
(10) Rodriguez, F. *Principles of Polymer Systems*, 2nd ed.; McGraw-Hill: Japan, 1983.
(11) Muller, G.; Lecourtier, J.; Chauveteau, G. *Macromol. Chem.* **1984**, 5.
(12) Ames, W. F. *Numerical Methods for Partial Differential Equations*, 2nd ed.; Academic: New York, 1977.
(13) Byrne, G. D.; Hindmarsh, A. C. *J. Comput. Phys.* **1987**, *70*, 1.
(14) Peaceman, D. W. *Fundamentals of Numerical Reservoir Simulation*; Developments in Petroleum Science 6; Elsevier: Amsterdam, 1977.
(15) Van Gnuchten, M. Th.; Alves, W. J. *Tech. Bull.-U.S. Dep. Agric.* **1982**, bulletin no. 1661.

Notes

Poly(crown ether): A Potential Candidate for Solid-State Electrolytes

DARMASENA PERAMUNAGE, JACK E. FERNANDEZ,* and L. H. GARCIA-RUBIO

Departments of Chemistry and Chemical Engineering, University of South Florida, Tampa, Florida 33620.
Received September 7, 1988; Revised Manuscript Received November 22, 1988

For the past few decades various classes of solid-state electrolytes have been extensively investigated. They include crystalline species such as β-alumina[1] and glasses such as $LiAlSiO_4$.[2] Recently the discovery of fast ionic conductivity in complexes such as poly(ethylene oxide) with lithium ion has kindled worldwide interest in similar systems and their ion-transport properties.[3-22] Applicability of polymers as solid electrolytes is based fundamentally on their ability to solvate metal ions, thereby isolating them effectively from their anions and thus avoiding the formation of immobile ion pairs. Clearly the energy of solvation of the salt by the polymer should be large enough to overcome the lattice energy of the salt. In addition to lattice energy considerations, a number of other factors seem to be crucial for the complexation process:[5,6,23-25] The solvation process is facilitated by the presence of a large concentration of polar groups; the polymer has to be flexible, as indicated by a low glass transition temperature, so that polymer molecules can be spatially reorganized during complexation to form the best local geometry for effective solvation.

On several occasions, solvation of metal ions in a polymer solid electrolyte has been shown to be analogous to that in macrocyclic crown ethers.[13,24,25] However, the ion conductive properties of a polymer with crown ether pendant groups incorporated into the backbone have not been previously reported. In this study poly((hydroxymethyl)-16-crown-5 methacrylate) was investigated as a possible candidate for an organic solid-state electrolyte in which a polymethacrylate backbone bears a pendant crown ether. Ionic conductivity of the model polymer–$LiClO_4$ complex was demonstrated by direct current measurement on a cell with platinum and/or lithium electrode.

Scheme I

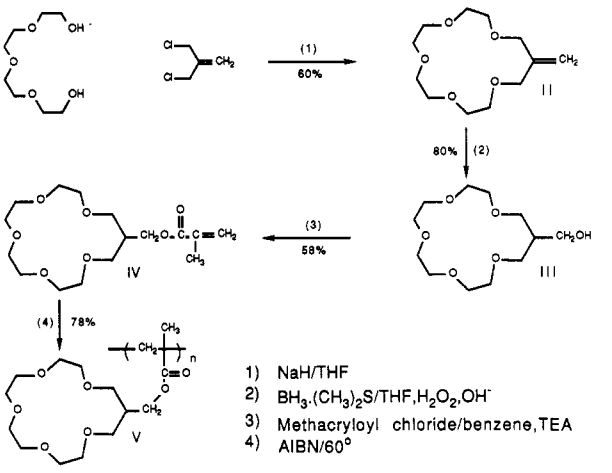

Experimental Section

A. Materials. Solvents were dried either with Linde 4A molecular sieves or CaH_2. AIBN was recrystallized twice from methanol. Tetraethylene glycol was vacuum distilled over anhydrous $CuSO_4$. 3-Chloro-2-(chloromethyl)-1-propene was purified by distillation and stored over molecular sieves. Methacryloyl chloride was prepared from methacrylic acid and benzoyl chloride as described previously[26] (yield 80%).

B. Synthesis of the Monomer. The synthetic procedure leading to the target polymer is outlined in Scheme I. (Hydroxymethyl)-16-crown-5 (III) (80% yield) was prepared from methylene-16-crown-5 (II) (60% yield), in turn prepared according to the method of Tomoi et al.[27]

16-Crown-5 methylenemethacrylate (IV) was prepared by first dissolving 14.0 g (5.3×10^{-2} mol) of III in 150 mL of dry benzene. After 75 mL of benzene was distilled off, the solution was cooled to ice temperature, and 19 mL of triethylamine (TEA) (0.13 mol) was added. To this solution was added 6.2 mL (6.36×10^{-2} mol) of methacryloyl chloride dropwise and with vigorous stirring over a period of 30 min. The reaction mixture was stirred for 2 h at

0024-9297/89/2222-2845$01.50/0